

A Framework for Aberration Compensated Displays

Fu-Chung Huang
Brian A. Barsky

Electrical Engineering and Computer Sciences
University of California at Berkeley

Technical Report No. UCB/EECS-2011-162

<http://www.eecs.berkeley.edu/Pubs/TechRpts/2011/EECS-2011-162.html>

December 21, 2011



Copyright © 2011, by the author(s).
All rights reserved.

Permission to make digital or hard copies of all or part of this work for personal or classroom use is granted without fee provided that copies are not made or distributed for profit or commercial advantage and that copies bear this notice and the full citation on the first page. To copy otherwise, to republish, to post on servers or to redistribute to lists, requires prior specific permission.

A Framework for Aberration Compensated Displays

Fu-Chung Huang and Brian A. Barsky

University of California, Berkeley

Computer Science Division

Electrical Engineering and Computer Sciences Department

Berkeley, CA 94720-1776

jonash@eecs.berkeley.edu

barsky@eecs.berkeley.edu

ABSTRACT

We are building upon our earlier work in Vision-Realistic Rendering, which is the computation of a displayed image that incorporates the characteristics of a particular individual's entire optical system. The key concept is, given the optical measurements of an individual's optical system, perform an "inverse blurring" computation on what would normally be displayed such that when this blurred version of the display is then viewed by this individual, it will appear in sharp focus when viewed by the individual whose optical system was used for this inverse blurring computation. There are two major impediments to performing inverse blurring: the generated image will have large, and even negative, values for some intensities, and some frequencies are lost after blurring. Building a high dynamic range display system will overcome the large/negative intensities problems. Introducing multiple layers of display with each layer located at a different viewing distance will overcome the lost frequencies. Next, there is the question of occlusion due to the multiple layers. One solution would be to use transparent displays, but if they cannot support high dynamic range imaging then an alternative is to construct a light-path-modulating system using mirrors to change the path of lights. The potential benefits are enormous for people who require vision correction, especially those whose optical problems include high-order aberrations since these aberrations are not corrected by eyeglasses. One application would involve construction of an "Aberration Compensated Display" in which the display would show images that have been transformed by inverse blurring individualized to the viewer such that when viewed by his or her optical system the resulting image will appear sharp. This will be useful for displays for computer monitors and hand-held mobile devices such as tablets and mobile phones.

1. Introduction

As the popularity of mobile hand-held devices continues to grow, a limiting factor that may emerge as an increasing impediment to their adoption among some sizeable segments of the population is the prevalence of vision problems. Effective use of these devices is predicated upon reasonable visual performance by a user who must interact with a small area. This is particularly problematic for the population of older users for whom there is a high prevalence of presbyopia and who face increasing incidence of other vision ailments as they age. But even for younger people, there is evidence that the prevalence of myopia is increasing, especially in Asian populations [Chew, 1994]. The emergence of the huge market of Asia is especially relevant since the prevalence of myopia, which varies by country and ethnic group, is approaching 70-90% in some Asian populations [Wong, 2000][Takashima,2001]. Furthermore, it is important to note that some visual impairments involve higher order optical aberrations (sometimes referred to by the less scientific term "irregular astigmatism"), which are impossible to correct with spectacle lenses; thus, this work could provide the opportunity to use mobile hand-held devices for the first time to those for whom this has been heretofore impossible due to their suffering from these ocular conditions. Moreover, using the built-in camera, a hand-held mobile device could be used to produce an "inverse-blurred" version of what the camera sees so that the user could look at the display and perceive a sharp image. The results of this approach would provide a tool for vision correction for people whose vision cannot be corrected with eyeglasses.

Over the past several years, we introduced and developed the concept of *vision-realistic rendering* [Barsky,2004], which is the computation of a displayed image that incorporates the characteristics of a

particular individual's entire optical system. Specifically, we developed a method for simulating the vision of actual human subjects based on their optical aberration data measured on a wavefront aberrometry instrument by an eye care clinician. Using our algorithms, we can create and display a synthetic image that incorporates the optical aberrations of an individual.

Our approach begins by measuring a subject's optical system by a Shack-Hartmann wavefront aberrometry device. This device outputs a measured wavefront which is sampled to calculate a PSF (PSF). The PSF is then used to blur input images. This blurring is accomplished by creating a set of depth images, convolving them with the PSF, and finally compositing to form a vision-realistic rendered image that simulates the vision of the individual whose optical system has been measured by the aberrometer.

With this backdrop, an intriguing question emerges: given the measurements of the optical aberrations spectacles prescription of a particular user, could his or her mobile hand-held device produce an altered image such that when it would be viewed by this user, it would appear in sharp focus to the user? That is, given the optical measurements of an individual's optical system, could the device perform an "inverse blurring" computation on what would normally be displayed such that this blurred version of the display would appear in sharp focus when viewed by the individual whose optical system was used for this inverse blurring computation?

The goal is to achieve vision correction algorithmically and digitally rather than optically; that is, given a user with refractive error corrected by spectacles or with high order optical aberrations, compute an individualized "inverse blur" transformation to be applied to a sharp image such that when the resulting transformed image is then viewed by this individual, the inverse blur is canceled by the optical aberrations of his or her vision and this blurred version of the image will appear in sharp focus to this individual. More specifically, the concept is to determine a special Point-Spread Function (PSF) based inverse blurred image such that when this is viewed by the individual whose optical aberrations are characterized by this PSF, the resulting image appears to be sharp. The concept is that when a person views the displayed image, the inverse blur will be cancelled by the blurring introduced by the optical aberrations of the individual.

This situation is complicated by the fact that the blurring PSF depends on the distance from the aberrations. However, for simplicity of derivation, we first assume that these factors are controlled.

This blurring process can be expressed mathematically as follows: The sharp image I^{clear} can be written as the result of the inverse blurred image I^{pre} (denoting "pre-compensated") convolved with the blurring kernel K that represents the individual's PSF. From this, the inverse blurred image can be expressed as the result of the sharp image convolved with the inverse of the blurring kernel.

$$I^{clear} = I^{pre} \otimes K, \text{ where } I^{pre} = I^{clear} \otimes K^{-1} \quad \text{eq. (1)}$$

Applying the inverse kernel to the sharp image produces the inverse blurred image whose blur will be cancelled by the optical aberrations of the individual whose PSF was used to form the kernel. Note, however, that this assumes that it is always possible to compute the inverse kernel. It is interesting to note that this is not always possible in general. However, we can proceed undaunted to make headway into solving this for many cases.

Inverse blurring comprises two steps: analyze the refractive error and then use that to inverse blur the image. The subject's optical system is measured using a Shack-Hartmann wavefront aberrometer, and then the blurring kernel that represents the individual's PSF is determined.

Other researchers attempting to perform inverse blurring [Alonso et al. 2004, Brown et al. 2006, Oyamada and Saito 2007] borrowed de-convolution methods from image de-blurring, but the results were unsatisfactory with low-contrast, ringing, and blurry artifacts.

We will first explain how these methods are applied and show the unacceptable artifacts. Then, we provide a thorough analysis of the fundamental differences in the problem formulations, and highlight the difficulties. Our approach is a new optimization-based framework that captures the power of integrating across **multiple images** to solve the problem of the artifacts.

This technique of integrating across multiple images is traditionally used in display super-sampling [Damera-Venkata, 2009] and display resolution enhancement [Didyk et al., 2010]. Using this approach, we are able to demonstrate improved quality of images compared to using single image de-convolution. We believe this system is more complete and will prove useful for vision correction, especially for those patients whose eyes have aberrations that are not correctable optically with spectacles.

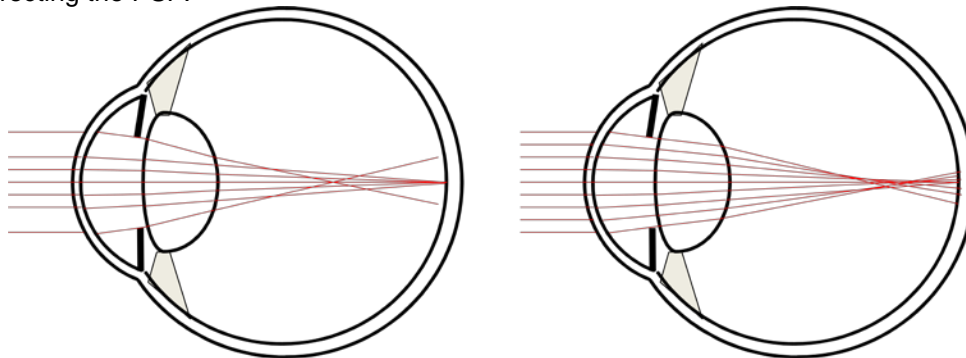
2. Background

The dynamic range of the focusing power of the crystalline lens of the human eye is huge: given a normal eye with 10Ds (diopters) of accommodating range, the eye can correctly focus from as close as 10cm to infinity. Having a properly focused image on the retina depends on the proper functioning of many different elements: the cornea, which performs 2/3 of the refraction, or bending of light, which is necessary to focus the image; the lens, which performs the remaining 1/3 of the refraction, stretched and squeezed by the ciliary muscles that can change its shape; finally the tear film, aqueous humour, and vitreous humour, which provide a medium through which the light can pass unperturbed.

Not all people reap the benefits of this complicated design. Throughout the world, hundreds of millions of people have vision problems that leave them unable to see with good acuity.

This research is concerned with the refractive elements of the eye and the errors or artifacts produced in the process of focusing light onto the retina. Any imperfect optical system produces such artifacts; they are known as aberrations. In optics, we distinguish between “low order” aberrations and higher order aberrations.

To see how the higher order aberrations occur, consider spherical aberrations, as illustrated in Figure 3(a). This type of aberration arises because the optics of the eye are not perfectly spherical, inducing higher focusing power off the optical axis. Unfortunately almost everyone has some of this aberration, resulting in a non-zero mean error among the human population. A more complicated optical system is shown in Figure 3(b): the blur has an irregular distribution, which is an impediment to measuring and correcting the PSF.



(a) Spherical Aberration

(b) Arbitrary Aberration

Figure 3: Higher order aberrations of the eye. (a) Spherical aberration with off-optical-axial rays focusing in front of the retina. (b) Irregular refraction causing an asymmetric and irregular PSF. The irregularities in the converging light cannot be corrected with spectacles; we are developing an algorithmic solution to inversely correct these phenomena in advance of the image formation in the eye.

In addition to occurring naturally in ocular conditions such as keratoconus, higher order aberrations are also a frequent side effect of LASIK surgery. LASIK is designed to reduce low-order aberrations by ablating the cornea. The wound heals with irregularities, which introduce new higher order aberrations that had not been present prior to the surgery. These problems are exacerbated in low light when the pupil size is larger than the treatment zone, causing glare, which can impair the vision quality of the patient.

3. Wavefront Aberrations

3.1. Wavefront

The wavefront is the surface that is perpendicular to the light rays that are at the same phase. When these rays are parallel to each other, then the wavefront for these rays is a plane, as shown in Figure 4(a). When the rays converging to a single point, a typical result of a biconvex lens, then the wavefront forms a spherical surface, as shown in Figure 4(b). In a perfect eye, parallel rays would converge to a point on the retina, resulting in a PSF that is a delta function; in this case, the combined optical system of the eye (anterior surface of the cornea, 2nd surface of the cornea, and crystalline lens)

converges these rays and is said to have positive refractive power. When the refractive power to converge these rays is too large; the focal point will be in front of retina, which is called myopia (nearsightedness in common parlance). In this case, corrective spectacles have negative power to diverge the rays before they enter the eye. This is analogous to our method, insofar as the eyeglasses solve the problem optically, whereas we solve it algorithmically. A more complicated situation arises when the optical system of the eye has irregularities, as shown in Figure 4(c); in this case, there may be no single focal point, an irregularly shaped wavefront, and a non-trivial PSF.

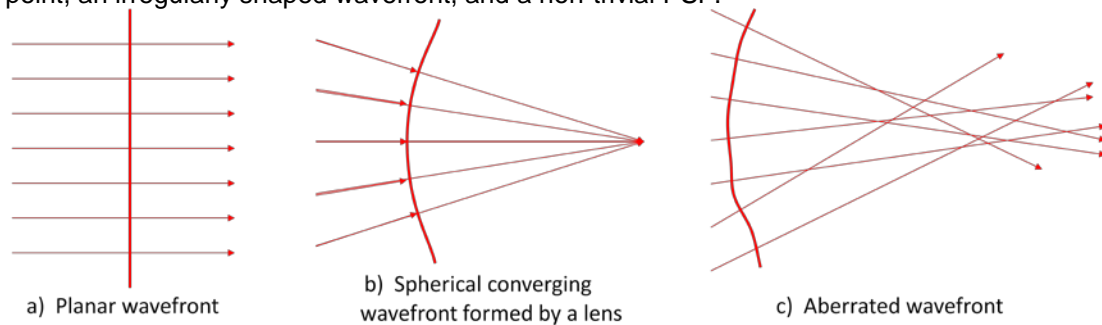
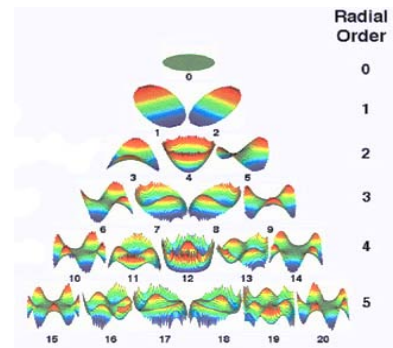


Figure 4: Illustration of different wavefronts. (a) Planar wavefront from parallel rays. (b) Spherical wavefront from converging rays. (c) Complex wavefront from irregular shaped refractive media.

3.2. Wavefront Decomposition with Zernike Polynomials

The wavefront of the individual can be measured using a Shack-Hartmann wavefront sensor. By analyzing the wavefront with Zernike polynomial functions, we can understand how the irregularities are formed.

Zernike polynomials are a set of basis functions used to describe a circular surface, $Z=W(x,y)$, a function useful to describe the wavefront surface of rays entering/exiting the circular pupil of the eye. The key property of Zernike polynomials is the decomposition of the shape function $W(x,y)$ into a frequency-series expansion of linear independent basis functions. The frequency decomposition is also common in computer graphics, e.g. spherical harmonics or wavelets. Using a series expansion, different kind of aberrations can be expressed in terms of frequency coefficients, in their radial orders. The expansion series is shown in the figure on the right.



The 0th order aberration is called “piston” and the two 1st order aberrations are called vertical and horizontal “prism”; they only shift and tilt the image. The aberrations of order 2 and above affect the quality of human vision, causing a PSF that is no longer a delta function.¹ The 2nd order aberrations are called “defocus” and vertical and horizontal “astigmatism.” They are the most common aberrations for the majority of people and fortunately are correctable via spectacle lenses.

The higher order aberration terms are those of order 3 and above. These are more complicated and include aberrations called “trefoil”, “coma”, “quadrafoil”, “spherical aberration” as well as many others that do not have names but are referred to only by mathematical expressions. Higher-order aberrations are traditionally hard to measure, and impossible to correct with spectacle lenses.

Although contact lenses have the potential to correct higher order aberrations, many eyes that exhibit higher order aberrations have corneas with an irregular surface shape that can prevent the successful fitting of a contact lens. Also, patients with presbyopia, that is, who require reading glasses, present still further challenges for satisfactory contact lens wear. For people whose vision involves higher order aberrations, it can be an ongoing struggle attempting to attain adequate vision correction.

¹ Actually there is no delta PSF; the best case is still diffraction-limited.

3.3. Wavefront and Point Spread Function (PSF)

After obtaining wavefront data, the PSF is computed given the pupil size as follows:

$$PSF(x, y) = FT\{P(x, y)\} = FT\left\{A(x, y)e^{-i\frac{2\pi}{\lambda}W(x, y)}\right\}$$

where the PSF is given by the Fourier transform of the pupil function, a composition of amplitude function $A(x, y)$ for light passing through certain pupil size, and the interferograms from all possible pair of points across the wavefront surface $W(x, y)$. An example of transformation from wavefront of 5mm pupil to its PSF on the retina is given below in Figure 5.

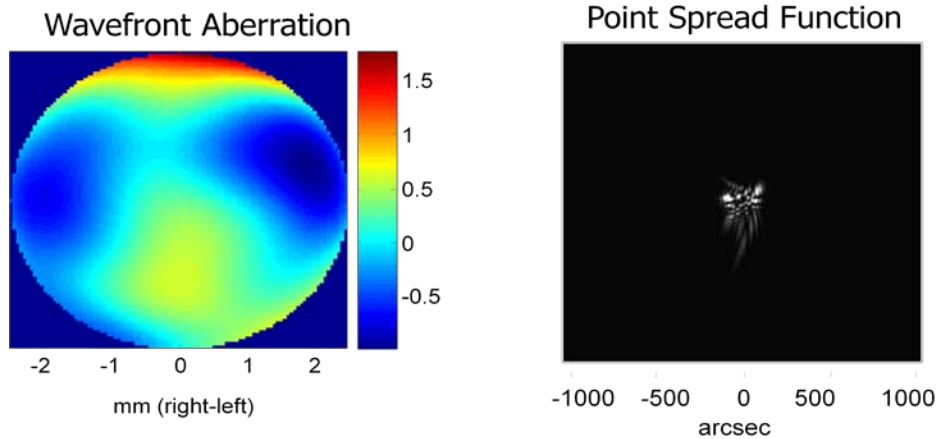


Figure 5: Wavefront aberration and its analytically derived PSF. *Left: The measured wavefront aberration from the pupil, with higher value indicating light goes faster, and vice versa. More complex color plots means more terms from higher order are involved. Right: The analytically derived PSF from the wavefront aberrations on the left. Unlike the lower order aberrations, whose PSFs are mostly circular or ellipsoid, the higher order aberrations usually exhibit non-trivial shaped PSF.*

Once the PSF is calculated, we want to use it for inverse blurring. Given the measured wavefront and PSF, we must modify the displayed image in advance so it cancels with the later blurring by the eye. In the following sections, we will give an overview of previous attempts, analysis of their pros and cons, and then our new framework.

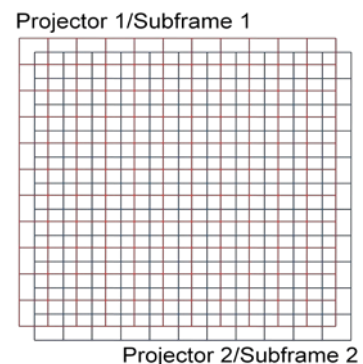
4. Related Work

Although our goal is to generate an inverse blurred image that will appear sharper when blurred by an individual's optical system, the overarching concept is similar to image de-blurring. Image de-blurring can be classified into "blind" and "non-blind," corresponding to whether the blurring kernel is taken into account or not.

For blind de-convolution, a thorough treatment of recent developments using MAP based estimators is provided in [Levin, 2009]. The trend is to use natural image statistics and marginalization over the entire image. The approach is to first robustly identify the blurring kernel and then apply standard non-blind de-convolution techniques, such as the Lucy-Richardson [Lucy, 1974] [Richardson, 1972] method or Wiener filter [Wiener, 1964].

These methods are appropriate and specifically designed for camera-shake blur, by assuming a smaller or Gaussian-like kernel and the prior of sparse derivatives about the unknown sharp image. However, these approaches are not usually directly applicable to the inverse blur problem.

The inverse blur problem is also related to projector display calibration and sharpening. [Brown et al., 2006] and [Oyamada and Saito, 2007] use the inverse filtering method (Wiener filter) to inversely blur images to eliminate artifacts caused by projecting an image on a tilted wall. These efforts are similar to our preliminary work, but they specifically apply to cases that involve a defocused



projection and estimation of PSF's. A similar problem is also addressed by [Grosse et al., 2010] who use a coded aperture on the projector, but this has the shortcoming of reduced light throughput.

Special insights about defocus blur were discussed in [Yellott and Yellott, 2007]. Specifically, the defocus blur introduces phase reversal in the frequency domain. The problem of spurious resolution occurs exactly at the location of reversal. The authors propose a solution similar to ours by pre-compensating the displayed image by considering the inverse of phase reversal which then cancels the spurious resolution effects with the defocus blur. However, the results still exhibit loss of high frequency information, and solutions are limited to low-contrast images. Although their method does not specifically address our problem, the insight into frequency content and the discussion about low-contrast results are valuable to us.

Recent work on display super sampling uses a technique called *wobulation* [Allen and Ulichney 2005] to increase perceived resolution. Multiple low-resolution projectors are aligned with slight shifts at the sub-pixel level, and the super-imposed projection can deliver higher resolution than the original projectors, as shown on the image at the right. The resolution and frequency increases are thoroughly discussed by [Damera-Venkata and Chang, 2009]. The insight in the paper is their mathematical proof of the validity; the high resolution image indeed exceeds the Nyquist rate of the low resolution images. The technique, although not directly related to de-convolution, provokes new thoughts and lays a foundation for our novel framework by restoring the lost higher frequency information.

To enhance the apparent resolution of a single display device, the idea regarding display super sampling is further extended by [Didyk et al., 2010]. The basic idea is to trade temporal sampling resolution for spatial resolution. Without multiple projectors, they use a high refresh rate monitor. By forcing the eye to move slowly within a sub-pixel level through Slow Pursuit Eye Motion (SPEM), pixel grids are shifted relative to the eye over time. On the high-refresh rate monitor, sub-frame images are superimposed and fused on the retina within the eye's response time. The combination of SPEM and time integration with a high refresh rate monitor enables the user to perceive even finer differences than the capability of the display device. A major artifact occurs when each sub-frame image has a refresh rate lower than the critical flicker frequency (CFF) of the eye, in which case a human subject will notice annoying flickering artifacts. The authors report a successful experiment with three sub-frame images on a 120Hz display monitor.

There is independent work by Alonso et al. that is closely related to some of our preliminary work described above in Section 5:

[Alonso and Barreto, 2004] use the Wiener filter for the inverse filtering solution, similar to our preliminary work. Their results suffer from the same artifacts that we reported above.

In [Alonso et al., 2005], the low-contrast problem is circumvented with a shifted rescaling grey level transformation to renormalize the image intensity, but problem is still present. Moreover, there is an inevitable blurring nature which is theoretically impossible to solve, as will be discussed in Section 7.2, which causes the low-frequency artifacts. The authors propose a frequency adaptive regularizer to lessen artifacts due to the lost frequencies.

A modified inverse filter is proposed in [Alonso et al., 2006] by thresholding magnitude of frequency bands below a very small magnitude. Noises and ringing artifacts introduced by such operations are further attenuated with Wavelet de-noising. However, a significant amount of information from high frequencies is also washed out, and the contrast problem still persists. The benefit of not choosing an appropriate parameter in Wiener filter is countered by additional two parameters in thresholding and Wavelet de-noising.

Finally, [Alonso et al., 2008] suggest an improved inverse kernel by introducing the diffraction-limited PSF into the Wiener filter to slightly smooth the results, and use post-extraction with image segmentation technique to better attenuate the rippling effects. However, complex background/foregrounds or images are difficult to handle, and the results still suffer from low-contrast and low frequency.

Alonso et al. have mainly focused on the deterministic Wiener filter with modification and post-processing to reduce artifacts. Our preliminary work explored a range of approaches including not only the Wiener filter but also the Maximum-A-Posteriori (MAP) based estimator as an "optimization based" framework.

5. Deconvolution and Inverse Blurring via Pre-Deconvolution

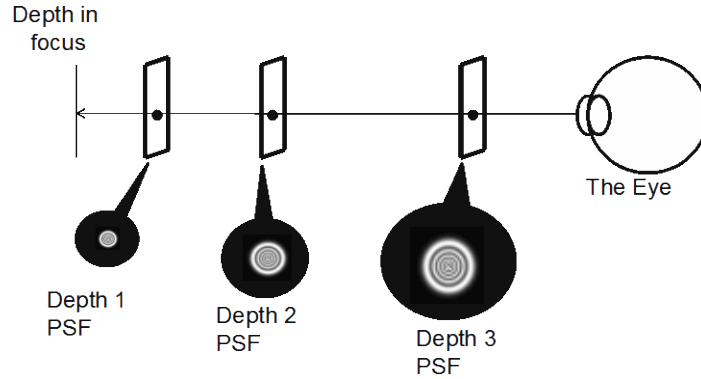


Figure 6: Scenario. Any point at a depth other than the depth-in-focus plane is defocused. Its defocus blur is characterized by its PSF. The farther away the points are located from the plane, the larger the blur is, and the higher is the loss in frequency information.

Consider the defocused lens configuration depicted in Figure 6 in which the eye is focused at a certain depth and any point at other depth is blurred and specifically characterized by a PSF or blurring kernel K . For any clear image I^{clear} placed at depth not in focus, the eye perceives the blurred image I^{blur} as:

$$I^{blur} = I^{clear} \otimes K \quad \text{eq. (2)}$$

Consider the inverse problem of image de-blurring which seeks to find the undistorted clear image given the blurred image and its blurring kernel. This problem can be approached in the frequency domain using a Wiener filter or in the spatial domain using the Richardson-Lucy iterative method.

Unfortunately, the blurring process nullifies some frequency bands, the zero-crossing frequency bands (as shown in Figure 8) and hence information is lost. Recent de-blurring methods use prior knowledge to recover the lost information by adding smooth or gradient distributions as regularization constraints.

Although de-blurring as a post-processing step may be useful to modify photographs, this approach cannot be applied to an image formed in the eye. Instead, it would be desirable to be able to do the processing in advance; that is, the idea would be to compute the preprocessed inverse-blurred image I^{pre} such that the inverse-blur cancels would cancel with the subsequent blur due to the optical aberrations (such as defocus) of the eye thereby producing a sharp image for the viewer.

We call this *inverse blurring* (or **pre-deconvolution**). Denoting the inversely-blurred image by I^{pre} , this can be expressed mathematically as:

$$\begin{aligned} I^{clear} &= \{I^{clear} \otimes K^{-1}\} \otimes K \\ &= I^{pre} \otimes K \end{aligned} \quad \text{eq. (3)}$$

There is a problem with the inversion process in that it tends to produce an image whose *dynamic range that is much larger than that of the original image*. This is due to a weak frequency response in the blurring kernel and division by weak response creates large values. There are usually many negative pixels and a bright spot in the inverse-blurred image.

Computation of the inverse-blurred image I^{pre} involves using inverse-filtering or a spatial domain solver. However, the situation is fundamentally different from that of performing the image de-blurring as a post-process. Since the blurring convolution is **the final step**, there is a *loss of frequency information* that cannot be recovered by adding prior knowledge. Thus, the left hand side of eq. (3) will not equate to the exact clear image. Therefore, even if we were to have a perfect deconvolution tool, the inverse blurring concept would still suffer from the nullifying process in these zero-crossing frequencies.

6. New Method

6.1. Two Problems

As described above, there are two problems with the inverse blurring concept: (1) large dynamic range of the inverse-blurred image, and (2) loss of frequency information. Our approach is to address the large dynamic range of the inverse-blurred image by using a high dynamic range (HDR) display system and the loss of frequency information by the concept of a *multi-layered display* that does not lose any frequency content even after the blurring.

6.2. Large Dynamic Range of the Inverse-Blurred Image

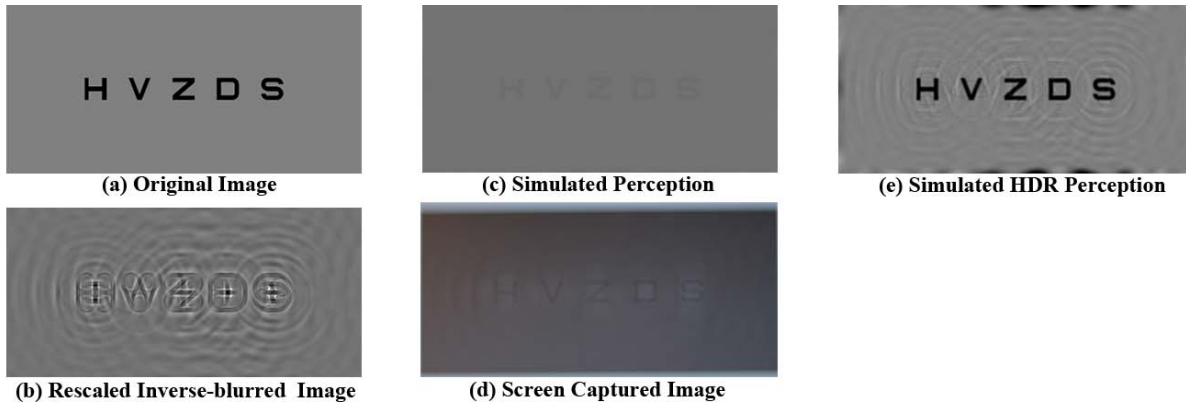


Figure 7: Single image inverse filtering. (a) Original sharp image. (b) Inverse-blurred image and rescaled. (c) Image then convolved with the blur to produce simulated perceived image. (d) Image from defocused DSLR camera capturing rescaled inverse-blurred image of (b). The low-contrast problems are apparent in images (c) and (d). This is due to the re-scaling on standard 8-bit display. If an HDR display were available, we could eliminate the re-scaling. (e) Simulated perceived image if HDR display were available. The contrast is restored but the image still suffers from ringing artifacts.

As noted in the previous section, the inverse blurring tends to produce an image with a larger dynamic range than the original image and, even worse, negative values for some intensities. The most common solution is to rescale the dynamic range of the inverse-blurred image to $[0,1]$, as is shown Figure 7(b). Prior to re-scaling, the inverse-blurred image has a dynamic range that is about 20 times that of the rescaled image. Consequently, when the rescaled inverse-blurred image is convolved with the blurring kernel K to form the perceived image, the resulting image (Figure 7(c)) has very low contrast compared to the original image (Figure 7(a)) for display on a standard monitor. Figure 7(d) shows the image from a defocused DSLR camera capturing the rescaled inverse-blurred image on a standard LCD monitor.

The low-dynamic range problem can be addressed by building a high dynamic range display system based on the idea in [Seetzen,2004] and [Bimber,2008]. The concept is to super-impose two display components: a projector onto either a LCD panel or a paper print. In theory, each of the two components provides 8-bits or 2^8 levels and then both together extend the brightness range to 2^{16} levels. Projecting onto a small area produces extraordinary brightness and thus the contrast ratio and brightness are greatly extended from a typical display. Although in theory the dynamic range of the inverse-blurred image is unbounded, we think that in practice the 16-bit display system should suffice.

Since the inverse-blurring process also tends to create negative pixel intensity, the overall intensity of the image is simply shifted so that the most negative value becomes zero. This constant intensity shift is, in general, compensated by the adaptation of the human visual system. The simulated blurring of the inverse-blurred image is shown in Figure 7(e). The dynamic range is greatly improved compared to Figure 7(c), but now significant ringing appears due to lost frequencies that are not recovered. In the next section, we will first describe the theory that gives full frequency spectrum response and then show a practical implementation.

6.3. Recovering the Lost Frequency Information

6.3.1. Frequency Response of a Single Image Filtering

In Figure 7, any point that is not at the depth-in-focus distance appears blurred, and the point has its PSF in the form of a disk². An image on that depth has a blurred projection on the retina corresponding to the original image convolved with the PSF.

In the 1D case, the out-of-focus blur is a box function with its magnitude of frequency response plotted as any one of the curves in Figure 8. Since the frequency response curves have many zero-crossings in their frequency domain, the retinal image is inevitably blurred due to the loss of information at these zero-frequency bands. As discussed at the end of Section 6, since the blurring convolution is the final step of the process, the problem will exist even with perfect inverse-blurring.

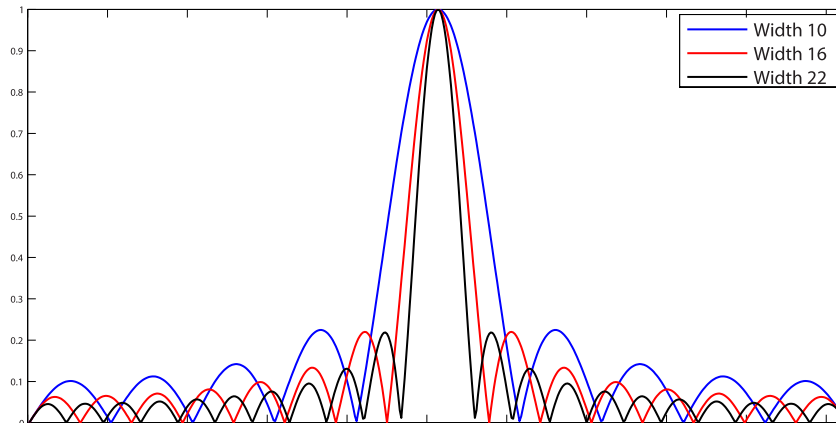


Figure 8: Frequency responses of PSFs under various defocused blurs. All frequency responses of the three defocused blurs have loss of frequency bands at their zero-crossings. The key insight is that the three defocused blurs have their zero-crossings mismatched; every frequency band has at least a blur with non-zero frequency response.

6.3.2. Multi-Depth Frequency Response

With careful inspection of the frequency response of the PSFs from all different depths (Figure 8), it can be observed that frequency spectra from different depths all have zero-crossings, but **at different frequency bands**.

The primary key insight is that we can find some depth combinations such that these zero-crossings do not coincide. In other words, for every frequency band, we can always find a non-zero frequency response from certain depths. If we were to separate the frequency bands of the image and display them at depths whose frequency responses are non-zero, then there will be no loss of frequency information.

In Figure 8, even though the user sees a blurred image at depth 1, the blurriness is compensated by images shown at depths 2 and 3. One problem, however, is the occlusion since it would not be possible to see more than one layer at the same time.

The second key idea in our approach is the temporal integration of the perceived retinal image. We will place transparent displays at the depth layers, as shown in Figure 7, and only activate one display at a time. We will cycle through each display monitor at a constant rate that is sufficiently high so as to be within the temporal integration time of retinal perception. This will require that every display have a high refresh rate. Using this approach, images from different depth layers will fuse to form a retinal image.

² The disk function is an approximation to the defocused kernel, but the frequency response is accurate up to the 3rd zero crossing.

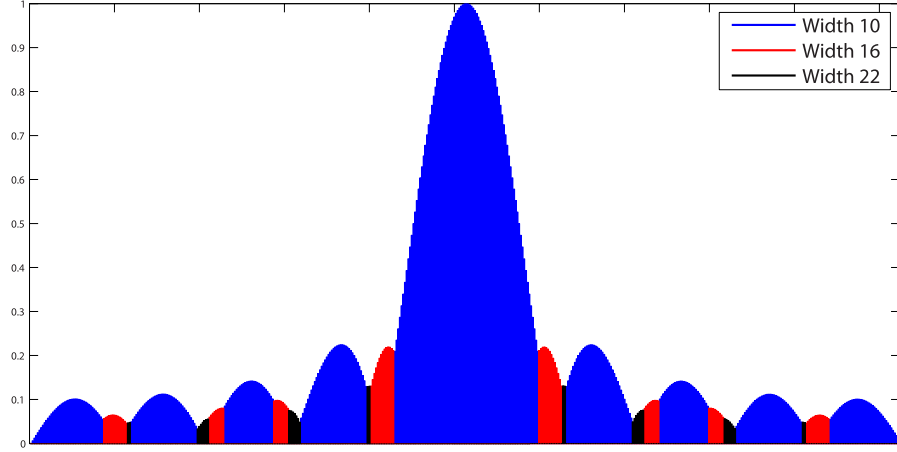


Figure 9: Frequencies assignment mask. Frequency bands from the image are assigned to display at different defocused distances according to the response properties, as in Figure 8. By carefully choosing the blurring kernel at each frequency, we can have non-zero spectral response and make the inverse problem well posed. In this figure, maximum frequency response is chosen.

To achieve the best quality and reduce superfluous dynamic range for the inverse-blurred image, we will use depths with maximal responses at each frequency band³. For the example of three depth layers as shown previously in Figure 8, we would assign a mask to the depth that has the highest frequency response, as shown in Figure 9.

The procedure can be summarized mathematically as integration in time over the retinal temporal response range Ω :

$$I_{perceived} = \int_{\Omega} PSF_{D(t)} \otimes IFT \left\{ \frac{M_{D(t)} * FT\{I^{clear}\}}{FT\{PSF_{D(t)}\}} \right\} dt \quad \text{eq. (4)}$$

where $D(t)$ specifies the depth index at any given time and the binary mask M assigns frequency bands to be displayed at depth $D(t)$. The ratio inside the inverse-Fourier-Transform is the inverse-blurring of the clear image given the PSF.

7. Implementation and Hardware Aspects of an Aberration Compensated Display

There are three key hardware aspects of our aberration compensated display system: high dynamic range, multi-depth layers, and high refresh rate.

In the previous section, we introduced the solution of a set of multi-layered transparent displays. However, this may conflict with the goal of high dynamic range because current state-of-the-art transparent displays lack a sufficiently high contrast ratio to support high dynamic range imaging.

There is a fallback solution similar to the construction by Jones et al. [Jones 2007]. Since the critical idea in the multi-layered depths display is depth-modulation, we will use mirrors to change the path of lights, as shown in Figure 10.

Using this approach, for the first half of the temporal integral, the lights will be reflected by the mirror on the turntable, and redirected to the HDR monitor. Then, by slightly rotating the mirror, the lights will be reflected to the second mirror, and then to the HDR monitor. Since the distance from the eye to the monitor determines the PSF, the mirrors create two paths of different lengths.

To enable seamless integration, the refresh rate of the HDR monitor will need to be at least 120Hz, and the turntable will rotate the first mirror at the same rate.

³ The maximal response may not be the best choice because at some frequency region, this tends to assign narrow bands to a depth layer, and cause large negative values. For video-based applications, we may want to maintain a steady constant intensity, and thus the presence of negative values and their associated constant intensity shift is important.

Mechanical issues can be avoided by using a birefringent (double refractive) prism and polarization rotating plate construction, similar to the birefringent lens used in [Love, 2009], to modulate the path electrically.

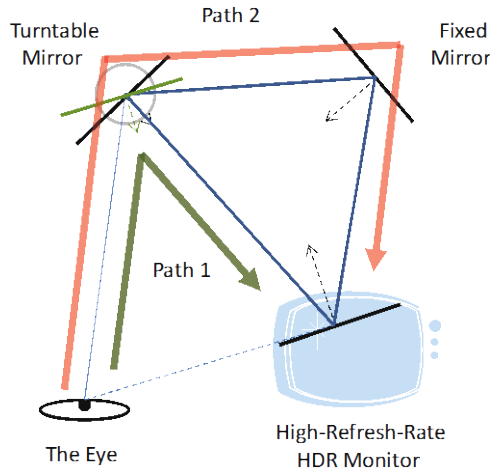


Figure 10: Mirror-based Configuration. The key component of our full-spectral response is the layered-depth display. We use a light-path modulating mirror to mimic the layers. For the first $1/120$ second, the lights follow path 1; for the next $1/120$ second, the mirror rotates so that the path is lengthened, thus creating another blurring kernel. The mirror can also be replaced with a birefringent prism.

8. Simulation Results

8.1. Synthetic Data

To illustrate how our approach operates in the standard 2D setting, we set up three layers of depth with disk PSFs whose diameters are 21, 29, and 37 pixels, respectively. We first find the frequency mask for different layers, as in Figure 12(a). The dark areas are frequencies assigned to the smallest PSF, whereas the white areas are assigned to the largest PSF.

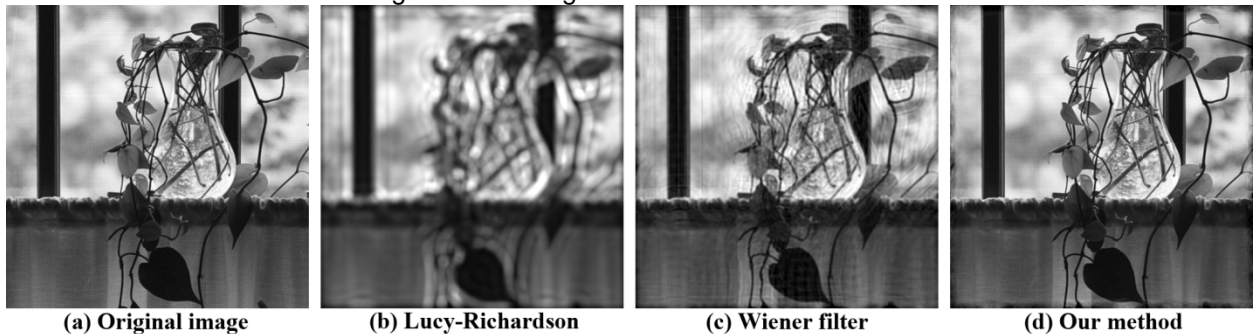


Figure 11: Comparison of simulated perceived results using different methods on an HDR display. Although the Wiener filter performs better than the Richardson-Lucy method, it produces ringing artifacts whereas our multi-layered defocused image does not lose any frequencies at all, and looks identical to the original image.

We use the image in Figure 11(a) for a test. Figures 12(b), (c), and (d) show the three images resulting from first inverse-blurring, then convolving with the respective blurring kernel, and finally re-scaling. The darkest region in Figure 12(a) corresponds to the smallest blur, which preserves the most frequency bands and is assigned to most of the image content. The remainder of the assignment to other depths is only intended to compensate for the lost frequency bands, as shown in Figures 12(c) and (d), and hence shows less structure from the original image.

Figure 11 shows simulated perceived results using different methods on a high dynamic range display. For methods using a single image, the PSF with 21 pixels diameter is used. The Richardson-Lucy method is unable to exactly preserve the high frequencies in the inverse-blurred image, and since this information is lost, the convolved result appears blurred. The Wiener filter performs quite well, except

it produces ringing artifacts. The Richardson-Lucy method is not very well suited for the inverse-blurring problem. Our multi-layered defocused image does not lose any frequencies at all, and looks identical to the original image.

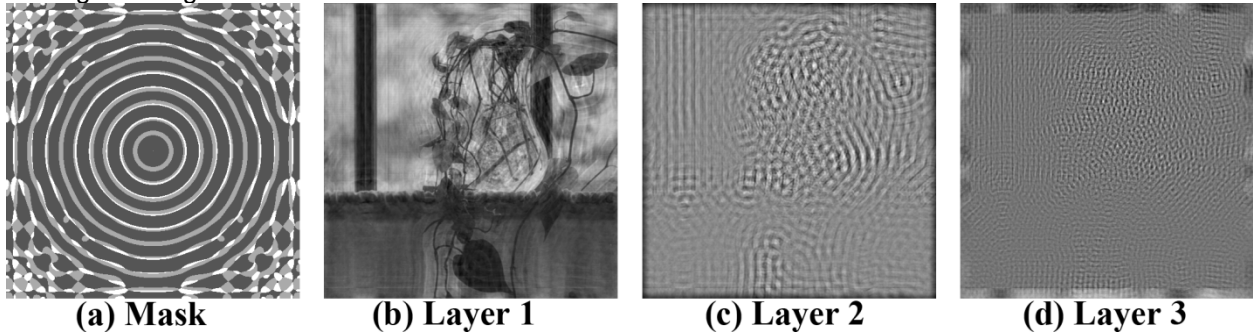


Figure 6: 3 Layer mask assignment for 2D frequencies. (a) Frequency bands assignment for 3 layers (b-d) Image perceived after the inverse-blurring and then the convolution with kernels, at depth 1, 2, and 3, respectively, with frequency bands assigned according to the mask in (a).

8.3. Higher Order Aberrations

As mentioned in Section 4.2, for people whose vision involves higher order aberrations, it can be an ongoing struggle attempting to attain adequate vision correction. However, the problem is the same as for the low order aberrations such as defocus blur using our multi-layered display framework. In fact, higher order aberrations are in principle even easier to solve because their blur is characterized by much more high frequency information, and the more high frequency responses, the easier the zero-valued frequency bands are covered by different depths.

9. Limitations of the Basic Method and Further Research

9.1. Noise model

The basic approach does not handle noise. For most image blurring processes, noise is added on the sensor side, which is the last step. Our inverse-blurring assumes no noise during the pre-processing and the later blur in the optical system of the eye.

9.2. Form Factor

Currently, the form factor of the system is determined by the size of the HDR display system which comprises an LCD panel, projector, and the light-path modulating unit. Even by carefully minimizing the depth-combinations, the HDR display component would still require a minimal projecting distance. In the future, if HDR displays become thinner, the form factor should become as thin as a tablet.

The ideal construction consists of multiple HDR transparent displays. Unfortunately, this is currently difficult to build because transparent displays are just now beginning to be commercially produced by Samsung, and they do not yet offer HDR capability. However, we can still proceed by instead using a construction based on stacking two 8-bit panels into one HDR panel, similar to the Layered 3D approach of [Wetzstein et al. 2011], yielding $8+8 = 16$ bits of intensity.

In the future, the advent of an HDR transparent panel will enable us to realize our approach of a multi-layered HDR transparent construction. Given a small thickness between layers (only a few millimeters), the ideal construction should have a similar form factor as the current LCD monitor/panel.

9.3. Sensitivity Analysis

In our inverse-blurring process, the frequency of the image is divided by the masked frequency of the blurring kernel, which is determined by the distance from the eye to the display. If the viewer shifts

without re-focusing, the image will cease to appear sharp. Since this is due to the change in the blurring kernel, we may try to dynamically update the blurring kernel using a tracking system.

Furthermore, since the multi-layered display also involves perspective projection, the later layers need to be enlarged by a scale factor to match the image in the previous layers. If the viewer moves, the scaling factor must be recalculated.

Other sources of instability are saccadic eye movements as well as unconscious accommodation (refocusing) of the lens of the eye. It might be interesting to investigate how to fixate the eye to stare at a specific location.

10. Conclusion

We are building upon our earlier work in Vision-Realistic Rendering, which is the computation of a displayed image that incorporates the characteristics of a particular individual's entire optical system. The key novel concept of our approach is, given the optical measurements of an individual's optical system, perform an "inverse blurring" computation on what would normally be displayed such that when this blurred version of the display is then viewed by this individual, it will appear in sharp focus when viewed by the individual whose optical system was used for this inverse blurring computation.

There are two major impediments to performing inverse blurring: the generated image will have large, and even negative, values for some intensities, and some frequencies are lost after blurring. Building a high dynamic range display system will overcome the large/negative intensities problems. Introducing multiple layers of display with each layer located at a different viewing distance will overcome the lost frequencies.

Next, there is the question of occlusion due to the multiple layers. One solution would be to use transparent displays, but if they cannot support high dynamic range imaging then an alternative is to construct a light-path-modulating system using mirrors to change the path of lights.

Eyeglasses cannot correct higher order optical aberrations that arise in the vision system of many patients who have corneal pathologies such as keratoconus or who experience side effects of corneal refractive surgeries (such as LASIK and PRK). Our results would transcend this limitation and provide vision correction for patients whose vision problems are related to either low or higher order optical aberrations. The ability to correct higher order aberrations is exciting since that is impossible to do with spectacles.

The common and simple task of looking at and reading a display screen is a struggle for patients whose vision suffers from high order aberrations, which are impossible to correct with spectacles. An **Aberration Compensated Display** would show images that have been transformed by inverse blurring individualized to the viewer such that when viewed by his or her optical system the resulting image will appear sharp. This will be useful for displays for computer monitors and hand-held mobile devices such as tablets and mobile phones. The increasing ubiquity of mobile hand-held devices presents a problem for users who lack reasonable visual performance; thus, our work could provide the opportunity to use mobile hand-held devices for the first time to those for whom this has been heretofore impossible due to their suffering from these ocular conditions

References

- AGRAWAL, A., XU, Y., AND RASKAR, R. 2009. Invertible motion blur in video. In ACM SIGGRAPH 2009 papers, ACM, New York, NY, USA, SIGGRAPH '09, 95:1–95:8.
- ALLEN, W., AND ULICHNEY, R. 2005. 47.4: Invited paper: Wobulation: Doubling the addressed resolution of projection displays. *SID Symposium Digest of Technical Papers* 36, 1, 1514–1517.
- ALONSO, M., J., AND BARRETO, A. 2003. Pre-compensation for high-order aberrations of the human eye using on-screen image deconvolution. In Engineering in Medicine and Biology Society, 2003. Proceedings of the 25th Annual International Conference of the IEEE, vol. 1, 556 – 559 Vol.1.
- ALONSO, M. AND BARRETO, A. 2004. An Image Processing Approach to Pre-compensation for Higher-Order Aberrations in the Eye. *SYSTEMICS, CYBERNETICS AND INFORMATICS*, Vol. 2, No. 3
- ALONSO, M., BARRETO, A. AND ADJOUADI M., 2008. Digital Image Inverse Filtering for Improving Visual Acuity for Computer Users with Visual Aberrations. *Inverse Problems in Science and Engineering*. Vol. 16. No 8, 957-966
- ALONSO, M., BARRETO, A., ADJOUADI M., AND JACKO, J. 2006. HOWARD: Higher-Order Wavefront Aberration Regularized Deconvolution for enhancing graphic displays for visually impaired computer users. *Lecture Notes in Computer Science*, vol. 4061, pp. 1163-1170
- ALONSO, M., BARRETO, A., ADJOUADI M., JACKO, J. AND CHOUDHURY M. 2005. Improving Computer Interaction for Users with Visual Acuity Deficiencies through Inverse Point Spread Function Processing. *IEEE SoutheastCon Conference*, Fort Lauderdale, FL, pp. 421-427
- BARSKY, BRIAN A. 2004. "Vision-Realistic Rendering: Simulation of the Scanned Foveal Image from Wavefront Data of Human Subjects", *First Symposium on Applied Perception in Graphics and Visualization*, co-located with ACM SIGGRAPH, Los Angeles, California, 7-8 August 2004, pp. 73-81.
- BIMBER, O., AND IWAI, D. 2008. Superimposing dynamic range. In ACM SIGGRAPH Asia 2008 papers, ACM, New York, NY, USA, SIGGRAPH Asia '08, 150:1–150:8.
- BROWN, M. S., SONG, P., AND CHAM, T.-J. 2006. Image pre-conditioning for out-of-focus projector blur. In *Proceedings of the 2006 IEEE Computer Society Conference on Computer Vision and Pattern Recognition - Volume 2*, IEEE Computer Society, Washington, DC, USA, CVPR '06, 1956–1963.
- CHEW, S.J., WEINTRAUB, J., RAJAN, U., TAN, F.T., AND CHAN, T.K. "Increasing prevalence of myopia in Singapore school children," In: Chew SJ, Weintraub J, editors. *Proceedings of the fifth international conference on myopia*, Toronto, Ontario, Canada, June 22-24, 1994. New York: Myopia International Research Foundation, 1995; pp. 41–46.
- DAMERA-VENKATA, N., AND CHANG, N. L. 2009. Display supersampling. *ACM Trans. Graph.* 28 (February), 9:1–9:19.
- DIDYK, P., EISEMANN, E., RITSCHER, T., MYSZKOWSKI, K., AND SEIDEL, H.-P. 2010. Apparent display resolution enhancement for moving images. In ACM SIGGRAPH 2010 papers, ACM, New York, NY, USA, SIGGRAPH '10, 113:1–113:8.
- FERGUS, R., SINGH, B., HERTZMANN, A., ROWEIS, S. T., AND FREEMAN, W. T. 2006. Removing camera shake from a single photograph. In ACM SIGGRAPH 2006 Papers, ACM, New York, NY, USA, SIGGRAPH '06, 787–794.
- GONZALEZ, R. C., AND WOODS, R. E. 2001. *Digital Image Processing*, 2nd ed. Addison-Wesley Longman Publishing Co., Inc., Boston, MA, USA.

GROSSE, M., WETZSTEIN, G., GRUNDHOFER, A., AND BIMBER, O. 2010. Coded aperture projection. *ACM Trans. Graph.* 29 (July), 22:1–22:12.

HONG, AARON, *Figure-Ground Saturation Preferences in Photographs*, Master's Research Project Report, Computer Science Division, Electrical Engineering and Computer Sciences Department, University of California, Berkeley, California, USA, August 2011.

JONES, A., MCDOWALL, I., YAMADA, H., BOLAS, M., AND DEBEVEC, P. 2007. Rendering for an interactive 360 light field display. In *ACM SIGGRAPH 2007 papers*, ACM, New York, NY, USA, SIGGRAPH '07.

LEVIN, A., FERGUS, R., DURAND, F., AND FREEMAN, W. T. 2007. Image and depth from a conventional camera with a coded aperture. In *ACM SIGGRAPH 2007 papers*, ACM, New York, NY, USA, SIGGRAPH '07.

LEVIN, A., WEISS, Y., DURAND, F., AND FREEMAN, W. 2009. Understanding and evaluating blind deconvolution algorithms. *Computer Vision and Pattern Recognition*, IEEE Computer Society Conference on 0, 1964–1971.

LOVE, G. D., HOFFMAN, D. M., HANDS, P. J., GAO, J., KIRBY, A. K., AND BANKS, M. S. 2009. High-speed switchable lens enables the development of a volumetric stereoscopic display. *Opt. Express* 17, 18 (Aug), 15716–15725.

LUCY, L. B. 1974. An iterative technique for the rectification of observed distributions. *The Astronomical Journal* 79 (June), 745+.

NAGAHARA, H., KUTHIRUMMAL, S., ZHOU, C., AND NAYAR, S. K. 2008. Flexible depth of field photography. In *Proceedings of the 10th European Conference on Computer Vision: Part IV*, Springer-Verlag, Berlin, Heidelberg, 60–73.

OYAMADA, Y., AND SAITO, H. 2007. Focal pre-correction of projected image for deblurring screen image. In *CVPR*.

RASKAR, R., AGRAWAL, A., AND TUMBLIN, J. 2006. Coded exposure photography: motion deblurring using fluttered shutter. In *ACM SIGGRAPH 2006 Papers*, ACM, New York, NY, USA, SIGGRAPH'06, 795–804.

RICHARDSON, H. W. 1972. Bayesian-Based Iterative Method of Image Restoration. *Journal of the Optical Society of America* 62, 1 (Jan.), 55–59.

SEETZEN, H., HEIDRICH, W., STUERZLINGER, W., WARD, G., WHITEHEAD, L., TRENTACOSTE, M., GHOSH, A., AND VOROZCOVS, A. 2004. High dynamic range display systems. In *ACM SIGGRAPH 2004 Papers*, ACM, New York, NY, USA, SIGGRAPH '04, 760–768.

SHAN, Q., JIA, J., AND AGARWALA, A. 2008. High-quality motion deblurring from a single image. In *ACM SIGGRAPH 2008 papers*, ACM, New York, NY, USA, SIGGRAPH '08, 73:1–73:10.

TAKASHIMA, T., YOKOYAMA, T., FUTAGAMI, S., OHNO-MATSUI, K., TANAKA, H., TOKORO, T., *et al.* "The quality of life in patients with pathologic myopia," *Japan J Ophthalmology* 2001; Vol. 45: pp. 84–92.

WETZSTEIN, G., LANMAN, D., HEIDRICH, W., AND RASKAR, R. 2011. Layered 3d: tomographic image synthesis for attenuation-based light field and high dynamic range displays. In *ACM SIGGRAPH 2011 papers*, ACM, New York, NY, USA, SIGGRAPH '11, 95:1–95:12.

WIENER, N. 1964. *Extrapolation, Interpolation, and Smoothing of Stationary Time Series*. The MIT Press.

WONG, T.Y., FOSTER, P.J., HEE, J., NG T.P., TIELSCH, J.M., AND CHEW, S.J., *et al.* "Prevalence and risk factors for refractive errors in an adult Chinese population in Singapore," *Invest Ophthalmology Vis Science* 2000; Vol. 41: p. S324.

YEH, CHE-HUA, NG, WAI-SENG, BARSKY, BRIAN A., AND OUHYOUNG, MING, "An Esthetics Rule Based Ranking System for Amateur Photos", SIGGRAPH Asia 2009 Sketches, Yokohama, Japan, 17-19 December 2009, Article 24, pages 1-1.

YEH, CHE-HUA, HO, YUAN-CHEN, BARSKY, BRIAN A., AND OUHYOUNG, MING, "Personalized Photograph Ranking and Selection System", ACM Multimedia 2010, Florence, Italy, 25-29 Oct. 2010, pp. 211-220.

YELLOT, J. I., AND YELLOT, J. W. 2007. Correcting spurious resolution in defocused images. *Human Vision and Electronic Imaging XII* (Feb.), p. -268.

YUAN, L., SUN, J., QUAN, L., AND SHUM, H.-Y. 2007. Image deblurring with blurred/noisy image pairs. In *SIGGRAPH '07: ACM SIGGRAPH 2007 papers*, ACM, New York, NY, USA, 1

YUAN, L., SUN, J., QUAN, L., AND SHUM, H.-Y. 2008. Progressive inter-scale and intra-scale non-blind image deconvolution. In *ACM SIGGRAPH 2008 papers*, ACM, New York, NY, USA, SIGGRAPH '08, 74:1-74:10.